Dynamics of the bacterial flagellar motor with multiple stators

Giovanni Meacci and Yuhai Tu[1]

IBM T. J. Watson Research Center, PO Box 218, Yorktown Heights, NY 10598

Edited by Howard C. Berg, Harvard University, Cambridge, MA, and approved January 2, 2009 (received for review October 3, 2008)

The bacterial flagellar motor drives the rotation of flagellar filaments and enables many species of bacteria to swim. Torque is generated by interaction of stator units, anchored to the peptidoglycan cell wall, with the rotor. Recent experiments [Yuan J, Berg HC (2008) *Proc Natl Acad Sci USA* 105:1182–1185] show that at near-zero load the speed of the motor is independent of the number of stators. Here, we introduce a mathematical model of the motor dynamics that explains this behavior based on a general assumption that the stepping rate of a stator depends on the torque exerted by the stator on the rotor. We find that the motor dynamics can be characterized by two timescales: the moving-time interval for the mechanical rotation of the rotor and the waiting-time interval determined by the chemical transitions of the stators. We show that these two timescales depend differently on the load, and that their cross-over provides the microscopic explanation for the existence of two regimes in the torque-speed curves observed experimentally. We also analyze the speed fluctuation for a single motor by using our model. We show that the motion is smoothed by having more stator units. However, the mechanism for such fluctuation reduction is different depending on the load. We predict that the speed fluctuation is determined by the number of steps per revolution only at low load and is controlled by external noise for high load. Our model can be generalized to study other molecular motor systems with multiple power-generating units.

torque–speed relationship | model | rotary | stepping statistics | speed fluctuation

The swimming motion of bacterium *Escherichia coli* is propelled by the concerted rotational motion of its flagellar filaments (1, 2). Each filament ($\sim$10 μm long) is driven by a rotatory motor embedded in the cell wall, with a angular speed of the order of 100 Hz (2). The motor has one rotor and multiple stators in a circular ring-like structure $\approx$45 nm in diameter (3). The stators are attached to the rigid peptidoglycan cell wall and the spinning of the rotor drives the flagellar filament through a short hook (see ref. 3 for a 3D reconstruction and Fig. 1*A* for a 2D sketch of the rotor-stator spatial arrangement). The rotor is composed of a ring of $\sim$26 FliG proteins and each stator has 4 copies of proteins MotA and 2 copies of proteins MotB, forming 2 proton-conducting transmembrane channels. A flow of protons (or, in some alkalophilic and marine *Vibrio* species of bacteria, sodium ions), due to electrochemical gradients across the channels, causes conformational changes of the stator proteins that generate force on the rotor through electrostatic interaction between MotA and protein FliG (4). The work per unit charge that a proton can do in crossing the cytoplasmic membrane through the proton channel is called the "proton-motive force" (*pmf*).

At any given time, a stator is engaged with one of the 26 FliG monomers on the FliG ring as the duty ratio of the flagellar motor is close to unity (5). Presumably, the passage of protons switches the stator to be engaged with the next FliG monomer on the FliG ring along the direction of rotation, stretching the link between the stator and the rotor. The subsequent relaxation process rotates the rotor and the attached load toward the new equilibrium position. This can give rise to a step-like motion, characterized by advances of the rotor followed by waiting periods. The molecular details of the flagellar motor has been the subject of intense research (2) and the step-like motion was recently demonstrated by direct observation (6) for a sodium-powered motor at very low *pmf*, but a general understanding of the stepping dynamics of a single flagellar motor is still lacking.

The torque-speed dependence is the key characteristics of the motor (2, 7, 8). The measured torque-speed curve [see Supporting Information (SI) *Appendix*] for bacterial flagellar motor shows two distinctive regimes. From its maximum value $\tau_{\max}$ at stall (zero angular velocity), the torque first falls slowly (by $\approx$10%) as angular velocity increases at up to a large fraction ($\approx$60%) of the maximum velocity, forming a plateau in the torque-speed curve. Then the torque starts to decrease quickly with increasing angular velocity, eventually approaching zero at the maximum velocity. For *E. coli* at room temperature under physiologically relevant conditions, the maximum angular velocity is $\approx$300 Hz and the estimated maximum torque ranges from 4,700 pN-nm (9) to 1,400 pN-nm (10, 11).

A few mathematical models (12–17) have been proposed to explain various aspects of the observed torque-speed characteristics based on assumptions about details of the electrostatic interaction between the stators and the rotor. In a more general approach, recent work by Xing *et al.* (18) has sought to understand the mechanism for the torque-speed curve characteristics without assuming a detailed description of the energy-transduction process. Their model can reproduce the observed torque-speed curve characteristics, and they suggested a set of general conditions to explain the observed torque-speed characteristics. However, the model by Xing *et al.* does not exhibit the correct behavior at low load. In their model, the maximum velocities depend inversely on the number of stators (see supporting information in ref. 18), whereas a recent experiment (19) shows that near-zero load the velocity of the motor is independent of the number of stators.

Here, we aim at understanding both the torque-speed relationship and the individual motor dynamics by using a simple model describing the rotor's mechanical motion and the stator's stepping probability. In our model, the stepping rate of a stator depends on the force between the stator and the rotor, in analogy to the Huxley model for Myosin (20). Specifically, "negative" force between a stator and its attached FliG monomer in the direction opposite to the rotation of the motor leads to a larger stepping rate for the stator. Under this general assumption, we find that the maximum velocity at (near) zero load in our model is mostly determined by the maximum stepping rate, independent of the number of stators, in agreement with the recent experiment by Yuan and Berg (19). Microscopically, the motor dynamics follows a repeated moving and waiting pattern characterized by 2 timescales: the moving-time interval t_m associated with the (mechanical) rotation of the rotor and the waiting-time interval t_w determined by the (chemical) transition of the stator. We find that t_m and t_w depend differently on

Author contributions: G.M. and Y.T. designed research, performed research, and wrote the paper.

The authors declare no conflict of interest.

This article is a PNAS Direct Submission.

[1]To whom correspondence should be addressed. E-mail: yuhai@us.ibm.com.

This article contains supporting information online at www.pnas.org/cgi/content/full/0809929106/DCSupplemental.

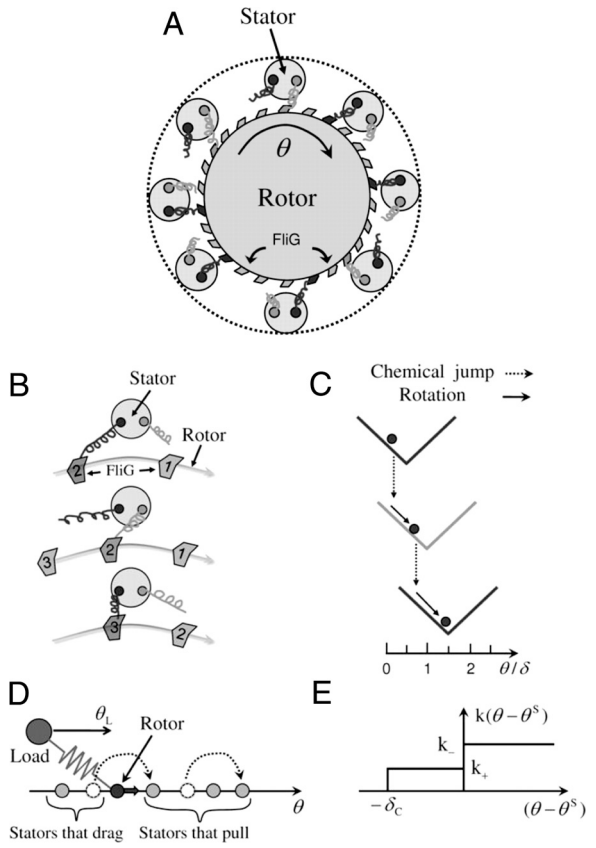

Fig. 1. A Model for the flagellar rotary motor. (*A*) Schematic illustration of the rotor–stators spatial arrangement. The rotor contains 26 FliG proteins and there are multiple stators, each with 2 subunits (dark and light springs). (*B*) A sequence of 3 rotor–stator configurations (from top to bottom) illustrating the hand-over-hand interaction between the 2 subunits of a stator and the FliG proteins in the rotor. (*C*) The same sequence as in *B* is shown in the potential landscape. The solid arrow represents the physical rotation of the rotor angle (θ) down a given (V-shaped) potential, the dotted arrow represents the chemical change (switching of hands) that shifts the potential. (*D*) The full motor model with multiple stators in the angle space. Each stator is represented by its internal angle θ^S. The rotor is pulled forward by the stators in front of it and dragged back by the stators behind it. The stator angle can only change by jumping forward with rate k that depends on the relative angle $\Delta\theta = \theta - \theta^S$. The form of $k(\Delta\theta)$ used in this article is given in *E*, which shows the dragging stators have a higher jump rate $k_- > k_+$ and a cutoff angle $-\delta_c$ where $k(\Delta\theta < -\delta_c) = 0$.

the load and their cross-over provides a natural explanation for the observed 2 regimes of the torque-speed curve. The fluctuation of the motor rotation is also studied in our model. We show that the sources of the motor speed fluctuation are totally different in the high- and low-load regimes and that the number of steps per revolution can only be extracted from the analysis of motor speed fluctuation in the low-load limit.

Model

In Fig. 1*A*, a schematic representation of a flagellar motor (rotor and stators) is shown. Each stator has 2 force-generating subunits symbolized by the light and the dark springs. The 2 force units of a stator interact with the FliG ring (rotor) in a hand-over-hand fashion as illustrated in Fig. 1*B*, analogous to the way kinesin proteins interact with microtubules (21, 22). The switching of hands (force-generating unit) represents the energy-assisted transition when one hand releases its attachment and the other hand establishes its interaction with the FliG ring (rotor). The forces between the FliG ring and the stators drive the rotation of the rotor. In Fig. 1*C*, the corresponding sequence of this hand-over-hand motion is shown in the energy landscape. The physical motion (solid arrow) of the rotor (circle) is governed by its interaction potential with the engaged FliG. The hand-switch transition (dotted arrow) corresponds to a shift of the potential energy in the direction of motor rotation by angle δ_0 and the subsequent motor motion is governed by this new potential until the next switch. Microscopically, the shift angle could be different for the front hand and the back hand (with respect to the direction of the motor rotation); here, for simplicity, δ_0 is a constant. Commensurate with the periodicity $\delta = 2\pi/26$ of the FliG ring, we should have $2\delta_0 = m\delta$ with a small integer m. In this article we choose $m = 1$ for simplicity.

Because of the small Reynolds number, the dynamics of the rotor angle θ and the load angle θ_L are overdamped and can be described by the following Langevin equations:

$$\xi_R \frac{d\theta}{dt} = -\frac{\partial}{\partial\theta}\sum_{i=1}^{N} V\left(\theta - \theta_i^S\right) - F(\theta - \theta_L) + \sqrt{2k_B T\xi_R}\alpha(t), \quad [1]$$

$$\xi_L \frac{d\theta_L}{dt} = F(\theta - \theta_L) + \sqrt{2k_B T\xi_L}\beta(t), \quad [2]$$

where ξ_R and ξ_L are the drag coefficients for the rotor and the load, respectively, and N is the total number of stators in the motor. V is the interaction potential between the rotor and the stator. V depends on the relative angular coordinates $\Delta\theta_i = \theta - \theta_i^S$, where θ_i^S is the internal coordinate of the stator i. θ_i^S increases by δ_0 when the stator switches hands. This discrete change in θ_i^S is called a jump of the stator in this article. The load is coupled to the rotor via a nonlinear spring described by a function F, which can be determined from the hook spring compliance measurement of ref. 23 (see *SI Appendix*, Fig. S1). The last terms in Eqs. **1** and **2** are stochastic forces acting on the rotor and on the load, with k_B the Boltzmann constant, T the absolute temperature, and $\alpha(t)$ and $\beta(t)$ independent white noise fluctuations of unity intensity.

The dynamics of the stator i is governed by the transition probability for the discrete jump of its internal variable θ_i^S during the time interval t to $t + \Delta t$: $P_i(\theta_i^S \rightarrow \theta_i^S + \delta_0)$. In this article, P_i is assumed to depend on the torque generated by the ith stator $\tau_i \equiv -V'(\Delta\theta_i)$, which depends on the relative angle $\Delta\theta_i$:

$$P_i\left(\theta_i^S \rightarrow \theta_i^S + \delta_0\right) = r(\tau_i)\Delta t = k(\Delta\theta_i)\Delta t. \quad [3]$$

The specific form of the jumping rate $r(\tau_i)$ [or $k(\Delta\theta_i)$] is unknown. We assume it to be a decreasing function of τ_i, with the stator stepping rate being higher when τ_i is negative ($\tau_i < 0, \Delta\theta_i > 0$) than when τ_i is positive ($\tau_i > 0, \Delta\theta_i < 0$).

Fig. 1*D* illustrates the motor dynamics, where the rotor (dark circle) is either pulled forward or dragged backward by individual stators (light circles) depending on their relative coordinates with respect to the rotor. The stator coordinate changes by jumping forward by δ_0 with a probability rate that is a function of its relative coordinate. For simplicity, we set the potential function V to be a V-shaped function: $V(\Delta\theta) = \tau_0|\Delta\theta|$, and the torque from a single stator is τ_0 with its sign depending on whether the stator is pulling ($\Delta\theta < 0$) or dragging ($\Delta\theta > 0$). Correspondingly, the stator jumping rate depends on the sign of the force: $k(\Delta\theta < -\delta_c) = 0$, $k(-\delta_c < \Delta\theta < 0) = k_+$, $k(\Delta\theta > 0) = k_-(> k_+)$ as illustrated in Fig. 1*E*. A cutoff angle δ_c is introduced to prevent runaway stators. Quantitatively, we use $\tau_0 = 505$ pN-nm, $\xi_R = 0.02$ pN-nm-s-rad^{-1}, $k_+ = 12{,}000$ s^{-1}, $k_- = 2k_+$, $\delta_c = \delta_0$ in this article unless otherwise stated. The load ξ_L varies from 0.002 to 50 pN-nm-s-rad^{-1}. Simulation time step $\Delta t = 0.01 - 1\ \mu s$.

Results

Two Characteristic Timescales and Their Different Dependence on the Motor Speed. In Fig. 2*A*, a typical case of time dependence of

the rotor angle $\theta(t)$ from our model is shown. The motion of the rotor consists of 2 alternating phases: moving and waiting. The moving phase occurs when the net force on the motor is positive (in the direction of motion). The waiting phase is when the system reaches mechanical equilibrium (net force equals zero) and the motions are driven by thermal fluctuation. The dynamics of the motor can thus be characterized by the 2 timescales t_m and t_w. The waiting-time t_w is the time the rotor spends fluctuating around a equilibrium position, i.e., the bottom of the total potential $V_t \equiv \sum_i^N V(\Delta\theta_i)$. Once in the waiting phase, the rotor can only start to have a net motion when a stator jumps to break the force balance and thus shift the equilibrium position forward. The subsequent net motion of the rotor to reach the new equilibrium position takes t_m, which is defined as the moving-time. The definitions of t_w and t_m are shown in Fig. 2*B*.

The dynamics of the motor depend on the load, the higher load leading to slower speed. We study how the 2 scales t_m and t_w vary with the load or equivalently the speed of the motor (speed is chosen because of its direct measurability in experiments). We find that the 2 time intervals have very different dependence on the motor speed as shown in Fig. 2*C*. The waiting-time interval is determined by independent chemical transitions, i.e, by a Poisson process with rate k, so we have: $\langle t_w\rangle \propto \langle k^{-1}\rangle$. Because k varies between 2 constants k_+ and k_- (except for extreme high load where $k = 0$), the averaged waiting-time has only a weak dependence on motor speed as shown in Fig. 2*C*. However, the average moving-time can be estimated as: $\langle t_m\rangle \approx \delta_m/\omega_m$, with δ_m the average angular movement, $\omega_m \equiv \tau_m/(\xi_R + \xi_L)$ the average speed, and $\tau_m \equiv \langle -V_t'\rangle_m$ the average net torque in the moving phase. Increasing the load ξ_L leads to a decrease of the speed ω_m and an increase of the moving-time. In addition, at lower speed, it is more likely for stators to jump in the middle of a moving phase before the system reaches its force equilibrium. These premature stator jumps effectively increase δ_m and further increase $\langle t_m\rangle$. These 2 factors lead to a strong dependence of $\langle t_m\rangle$ on the load (or the speed) as shown in Fig. 2*C*. Besides the difference in their average values, the distribution functions for t_m and t_w are also different (see *SI Appendix*, Fig. S2 for details).

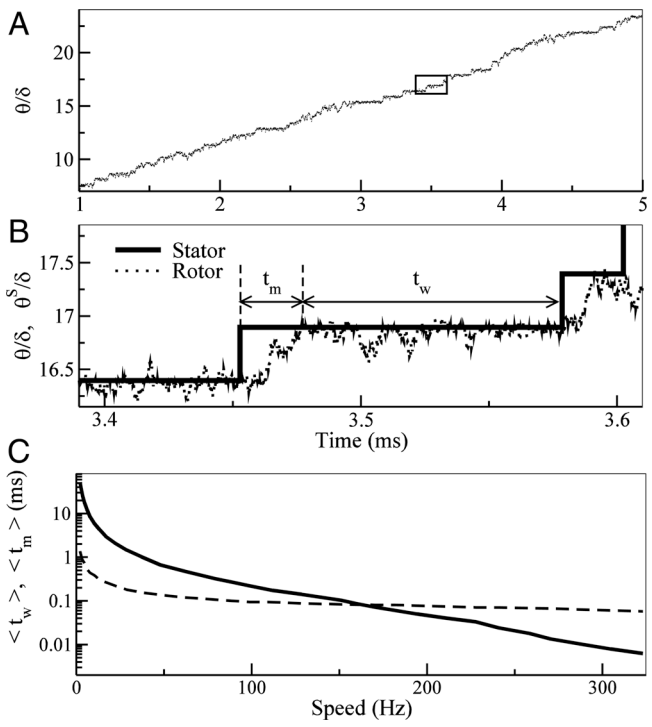

Fig. 2. The motor dynamics and its dependence on the load. (*A*) Rotor angle θ versus time for ~4/5 of a revolution for $N = 1$. The angular unit is the FliG periodicity δ. *Inset* is enlarged in *B*. (*B*) Zoom of the time series in *A* showing 2 complete steps. Solid line shows the stator position θ^S. A jump in θ^S marks the start of a moving phase for the rotor and the waiting phase starts when the rotor catches up with the stator. The definitions of the moving-time t_m and the waiting-time t_w are shown. (*C*) The average waiting-time $\langle t_w\rangle$ (dashed line) and the average moving-time $\langle t_m\rangle$ (solid line) over 500 revolutions as a function of the rotational speed for $N = 1$. $\langle t_w\rangle$ decreases slowly with increasing speed from 1 ms to 0.1 ms whereas $\langle t_m\rangle$ decreases much faster from ≈50 to 0.005 ms.

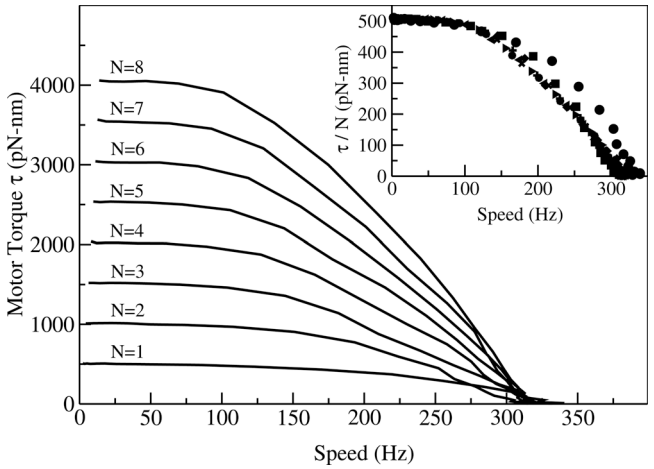

Fig. 3. The torque-speed ($\tau - \omega$) curves for different stator numbers ($N = 1$ to $N = 8$) from our model. Two regimes of the $\tau - \omega$ curves, i.e., constant τ up to a large knee speed ω_n and fast decrease of τ to zero at the maximum speed $\omega_{\max}$, are evident for all stator numbers. The torque per stator τ/N versus the speed ω is shown in *Inset*. The torque at stall scales with N whereas the maximum speed is independent of N.

The Two Regimes of the Torque-Speed Curve. In Fig. 3, the torque-speed curves calculated from our model for 8 different stator numbers are shown. Our model results closely resemble the observed torque-speed curves. There is a plateau regime with almost constant (10% decrease) torque from zero up to a large speed (≈100 Hz for $N = 8$), followed by a steep declining regime of the torque, all the way to zero at a speed of ≈300 Hz. By using the 2 timescales t_m and t_w, and noting that the net torque is zero during the waiting phase of the motor, the time-averaged torque τ and speed ω can be estimated:

$$\tau \approx \frac{\langle t_m\rangle}{\langle t_m\rangle + \langle t_w\rangle}\tau_m,\ \omega \approx \frac{\delta_m}{\langle t_m\rangle + \langle t_w\rangle}. \qquad [4]$$

The 2 distinctive regimes in the torque-speed curve can be understood intuitively within our model by the different dependence of $\langle t_m\rangle$ and $\langle t_w\rangle$ on the speed shown in the last section.

In the low-speed (high-load) regime defined by $\langle t_m\rangle \gg \langle t_w\rangle$, we have $\tau \approx \tau_m$ and $\omega \approx \delta_m/\langle t_m\rangle$ from Eq. **4**. As discussed in the last section, for low speed a stator can jump prematurely during the moving phase before the system reaches the bottom of the potential well. As a result, each stator spends most of its time generating positive torque τ_0. Therefore, in this high-load regime, although the speed changes significantly, the torque stays near its maximum value $\tau_{\max} = N\tau_0$, which is proportional to the number of stators.

In the high-speed (low-load) regime defined by $\langle t_m\rangle \ll \langle t_w\rangle$, we have $\tau \approx \tau_m\langle t_m\rangle/\langle t_w\rangle$ and $\omega \approx \delta_m/\langle t_w\rangle$ from Eq. **4**. As shown in Fig. 2*C*, for increasing speed $\langle t_m\rangle$ decreases quickly whereas $\langle t_w\rangle$ remains approximately the same. This naturally explains the steep decrease of the torque τ with speed in the high-speed regime. Intuitively, in this high-speed regime, a stator can be pushed into the negative-torque region ($\Delta\theta > 0$) because the rotor rotates too fast for the premature jump to occur. Because the stators spend

large fractions of their time dragging the rotor, the torque of the motor decreases quickly.

The different dependence of the waiting and moving-time intervals on the speed not only gives a clear general explanation for the 2 regimes of the torque-speed curve, it also explains the sharpness of the transition between the 2 regimes. Because the dependence of $\langle t_m \rangle$ on the speed is much steeper than that of $\langle t_w \rangle$ (as shown in Fig. 2*C*), the cross-over between the 2 regimes takes place in a small region of the speed values, thus making the 2 regimes in the torque-speed curve well defined, as found in both experiments and simulations of our model.

Independence of the Motor Speed on the Number of Stators at Near-Zero Load. At near-zero load, our model shows that the motor moves with an approximately constant speed that is independent of the number of stators, as demonstrated in Fig. 3. Recent resurrection experiments using gold nanoparticles (extremely low load) indeed showed such independence (19). The mechanism for this surprising behavior can be understood with our model. In the low-load regime, the motor spends most its time in the waiting phase where the net torque is zero. In our model with symmetric potential V, this force equilibrium is achieved by having on average half of the stators pulling the rotor and the other half dragging it. If we number the stators in Fig. 1*D* from left to right, the rotor's equilibrium position sits between the $N/2$th and the $(N/2+1)$th stators. This equilibrium state breaks under 2 possible scenarios: (*i*) One of the $N/2$ dragging stators jumps to the pulling side. This occurs with a probability rate $Nk_-/2$. (*ii*) The $(N/2+1)$th stator jumps and shifts the equilibrium to a position between the $N/2$th and the $(N/2+2)$th stator. This occurs with probability rate k_+. The average distances between the new and the old equilibrium positions are $\delta_m (\approx \delta_0/N)$ and $\delta_m/2$ for scenarios *i* and *ii*, respectively. The fundamental reason for the decrease in step size with N is due to the high duty ratio as first recognized in refs. 24 and 25. Similar step size reduction with N was recently observed in kinesin-1 motor (26). The maximum speed $\omega_{\max}$ near zero load is then:

$$\omega_{\max}(N) \approx \delta_m \frac{Nk_-}{2} + \frac{\delta_m}{2} k_+ \approx \frac{k_- \delta_0}{2}[1 + (k_+/k_-)N^{-1}], \qquad \textbf{[5]}$$

which only depends weakly on N, if $k_+/k_- \ll 1$. The estimated maximum speed $\omega_{\max} \propto k_- \delta_0/2$ makes sense as $\omega_{\max}$ should be limited by the step size and the maximum stepping frequency of an individual stator.

We have studied the dependence of $\omega_{\max}$ on the ratio $r \equiv k_+/k_-$ and N by numerical simulations of our model. In Fig. 4*A*, we show the torque-speed curves for $N = 1$ and $N = 8$ for 2 different values of r: $r = 0.2$ and $r = 1.2$. To quantify the dependence of $\omega_{\max}$ on N, we define a quantity $\Delta \equiv 2(\omega_{\max}(1) - \omega_{\max}(8))/(\omega_{\max}(1) + \omega_{\max}(8))$ to characterize the relative difference between the maximum speeds for motors with 1 and 8 stators. As shown in Fig. 4*B*, $\omega_{\max}$ is roughly independent of N, i.e., $|\Delta| < 0.1$ as long as $r \leq 0.5$. However, $\omega_{\max}(1)$ becomes significantly bigger than $\omega_{\max}(8)$ for $r \geq 1$. The observed dependence of Δ on r agrees well with the analytical estimate given by Eq. **5**.

Motor Speed Fluctuation at Different Load Levels and the Estimate of Step Numbers. The measured motor speed fluctuates because of 2 main factors: the external noise, such as the Brownian noise and measurement noise, and the intrinsic probabilistic stepping dynamics of the stators. Samuel and Berg (25) first investigated the speed fluctuations by studying the smoothness of the periodic motor motion characterized by $\Gamma \equiv n\langle T_1 \rangle^2/(\langle T_n^2 \rangle - \langle T_n \rangle^2)$, where T_n is the period for n revolutions. By measuring Γ in a resurrection experiment where the stator number is inferred from the discrete increments in average motor speed, it was found that Γ is proportional to the number of stators. The proportionality constant was interpreted as the number of steps per revolution. Here, we analyze the motor fluctuation by using our model to understand how different noise sources contribute to Γ and how Γ behaves differently at different load levels.

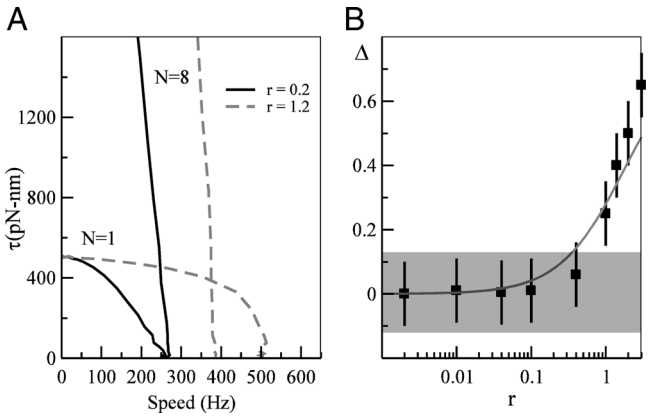

Fig. 4. Dependence of the maximum speed at zero load on N as a function of $r \equiv k_+/k_-$. (*A*) Torque-speed curves for $r = 0.2$ (solid lines) and $r = 1.2$ (dotted lines) are shown for $N = 1$ and $N = 8$. We change r by varying k_+ and keeping k_- constant. For $r = 0.2$, the maximum velocities $\omega_{\max}(1)$ and $\omega_{\max}(8)$ at zero load are roughly the same, but they differ significantly for $r = 1.2$. (*B*) The dependence of $\Delta = 2(\omega_{\max}(1) - \omega_{\max}(8))/(\omega_{\max}(1) + \omega_{\max}(8))$ on r. The line represents our analytical predictions from Eq. **5**. The shaded region shows the ~12% experimental error.

For low loads, the motor spend most of its time in the waiting phase. The average motor step size is $\delta_m \approx \delta_0/N (\ll 2\pi)$, there are $n_s \equiv 2\pi/\delta_m \approx 2\pi N/\delta_0$ steps in each revolution, and the average periodicity is $\langle T_1 \rangle = n_s \langle t_w \rangle$. Because the waiting-time intervals are uncorrelated, the variance of the n-revolution periodicity can be expressed as: $\langle T_n^2 \rangle - \langle T_n \rangle^2 = n n_s (\langle t_w^2 \rangle - \langle t_w \rangle^2)$. Furthermore, because the waiting-time t_w is determined by a Poisson process, its variance is equal to $\langle t_w \rangle^2$. Γ can thus be written as:

$$\Gamma \equiv \frac{n\langle T_1 \rangle^2}{\langle T_n^2 \rangle - \langle T_n \rangle^2} \approx \frac{n_s \langle t_w \rangle^2}{\langle t_w^2 \rangle - \langle t_w \rangle^2} \approx \frac{2\pi}{\delta_0} N, \qquad \textbf{[6]}$$

showing that $\Gamma = \gamma N$ is proportional to the stator number N, and the proportionality constant $\gamma = 2\pi/\delta_0$ corresponds to the number of steps per stator per revolution. This behavior is verified in our model by calculating Γ during a simulated resurrection process, where additional stators are added by a Poisson process with time constant $t_s = 400$ s (Fig. 5). For near zero load, the average speed is independent of the stator number in agreement with ref. 19 (see Fig. 5*A*). However, Γ increases by a fixed amount $\gamma = 2\pi/\delta_0$ as a new stator is incorporated into the system as shown in Fig. 5*B*, consistent with the analytical result by Eq. **6**. The behavior of Γ as shown in Fig. 5*B* represents a quantitative prediction of our model that could be tested in resurrection experiments with extreme low load, such as in ref. 19.

For high load, the net torque is roughly constant $\tau \approx N\tau_0$ and the speed can be expressed as $\omega_0 = \tau/(\xi_L + \xi_R) \approx N\tau_0/\xi_L$, which explains the constant increment of speed for every additional stator (up to eight) seen in our model (Fig. 5*C*) as well as in the resurrection experiments by Blair and Berg (27). For additional stators beyond a certain large number of stators, the speed passes the knee in the speed-torque curve and our model predicts a decrease in the speed increment, which is consistent with the recent experiments by Reid *et al.* (11) that showed the same decrease in speed increment as stator number goes up to $N = 11$. The dynamics of the load angle can be obtained by summing Eqs. **1** and **2** and taking the limit $\xi_R/\xi_L \to 0$. This leads to: $\theta_L = \omega_0 + \sqrt{2K_B T/\xi_L}\beta(t)$, which describes the simple motion of the load with a constant speed ω_0 perturbed by random noise. From the equation for θ_L, the periodicity and its variance can be determined: $\langle T_n \rangle \approx 2n\pi/\omega_0$, $\langle T_n^2 \rangle - \langle T_n \rangle^2 \approx 4n\pi k_B T/(\xi_L \omega_0^3)$. We can now express Γ as:

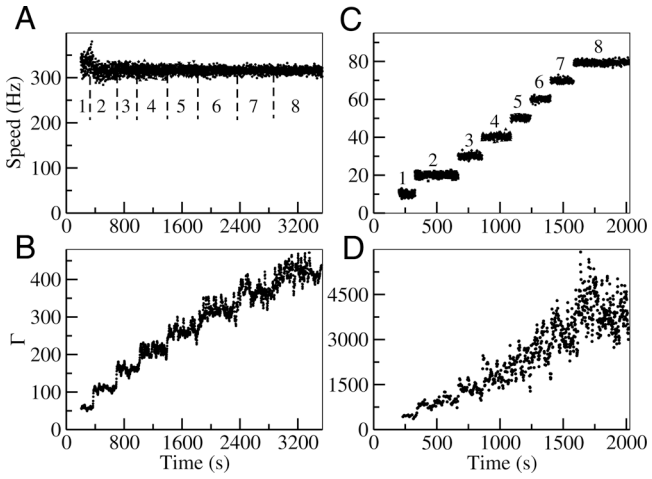

Fig. 5. The motor speed and its fluctuation in a simulation of the resurrection process for low and high loads. (*A*) Speeds as a function of time after successive stators are added at low load ($\xi_L = 0.002$ pN-nm-s-rad^{-1}). The simulation shows no dependence of the speed on the number of stator (labeled with a number from 1 to 8). (*B*) The smoothness parameter Γ with $n = 5$ calculated from the time series shown in *A*. Γ value is calculated with a moving-time window of 1.5 s (~500 revolutions). (*C*) Same as *A* at high load ($\xi_L = 8$ pN-nm-s-rad^{-1}) showing the approximately linear dependence of the motor speed ω on *N*. (*D*) Γ at high load from the time series shown in *C* using a window of approximately 10 s corresponding to a total of 100 revolutions. *B* and *D* show that Γ increases with *N* at both high and low load.

$$\Gamma \equiv \frac{n\langle T_1\rangle^2}{\langle T_n^2\rangle - \langle T_n\rangle^2} \approx \frac{\pi\xi_L}{k_BT}\omega_0 \approx \frac{\pi\tau_0}{k_BT}N. \qquad [7]$$

Γ is again proportional to N through its dependence on the speed ω_0. However, unlike in the low-load regime, the proportionality constant $\gamma = \pi\tau_0/(k_BT)$ has nothing to do with the number of steps per revolution. Instead, γ depends on the ratio between the intrinsic driving force (τ_0) and the external noise k_BT, as the driving force overcomes the external noise to make the motor moves smoothly. This behavior is verified in our model by calculating Γ during the resurrection simulation. As shown in Fig. 5*D*, Γ goes up with the number of stators but with a much larger proportionality constant γ, which quantitatively agrees with the expression $\pi\tau_0/(k_BT)$ from our analysis.

Therefore, although the motor-speed fluctuation is always suppressed by higher numbers of stators, the mechanisms are different for different load levels. For low load, the smoother motion for larger N is caused by the increase in step number per revolution. For high load, the smoother motion for larger N is caused by larger driving force (therefore larger speed) compared with the constant external noise. The difference in motor fluctuation between the high- and the low-load regimes is confirmed by our simulation as shown in Fig. 6, where the proportional constant Γ is shown for different values of external noise strength k_BT (Fig. 6*A*) and different load (Fig. 6*B*).

Summary and Discussion

We have presented a mathematical description of the rotary flagellar motor driven by hand-over-hand power thrusts of multiple stators attached to the motor. All key observed flagellar motor properties (2), including those from a recent resurrection experiment at near zero load (19), can be explained consistently within our model. The crucial ingredient of our model is that the hand-switching rate depends on the force between rotor and stator. This feature is known to be valid for other molecular motors, including kinesin (28) and myosin (29). Therefore, our model should be generally applicable to the study of these linear motors, especially in the case when there are multiple power-generating units attached to the same track (26).

For the flagellar motor, we find that its dynamics follows an alternating moving and waiting pattern characterized by 2 timescales t_m and t_w. The mechanism underlying the observed torque-speed relationship and its dependence on the number of stators is revealed by studying the dependence of these 2 timescales on the load. For high load, $\langle t_w\rangle \ll \langle t_m\rangle$, the motor spends the most time moving (albeit slowly) with all the stators pulling the motor in the same direction. So the torques generated by individual stators are additive, leading to an approximately constant torque $\tau_{max} \approx N\tau_0$, which persists up to the knee speed ω_n. Microscopically, the existence of this torque-plateau regime is due to the premature stator jumps that prevent the stators from going into the negative-torque region. Because the rate of the premature jumps is $k(\Delta\theta < 0)$, larger k_+ and larger cutoff δ_c increase the knee-speed ω_n (see *SI Appendix* Fig. S3 for details). For low load, $\langle t_w\rangle \gg \langle t_m\rangle$, the motor spends the most time in the waiting state. A waiting period ends when one of the dragging stators jumps to the pulling side or the pulling stator closest to the bottom of the potential well jumps. Therefore, the maximum motor speed ω_{max} is limited by the maximum jumping rate of the stators. ω_{max} can be estimated from our model. Eq. **5** shows that ω_{max} has only a weak dependence on N for small k_+/k_-, as confirmed by simulations of our model, and in agreement with recent resurrection experiments at near-zero load (19). Eq. **5** also explains the strong dependence of ω_{max} on N in a recent model by Xing *et al.* (18). The jumping probability used in ref. 18 has a complicated profile and is maximum in the positive-torque region. In our model, this would correspond to having $k_+/k_- \gg 1$, which is the opposite to what is required to achieve independence of ω_{max} on N.

The robustness of our results was verified by using different forms of the rotor-stator potential V and the force function F between the load and the rotor. In particular, we have studied a smoothed symmetric potential with a parabolic bottom and an asymmetric potential V (similar to the one used in ref. 18) where the negative torque (τ_-) is bigger than the positive torque (τ_+). We find that all of our general results remain the same (see *SI Appendix*, Figs. S4 and S5, for details). For the asymmetric potential, the condition for ω_{max} being independent of N is generalized to $k_+/k_- \ll \tau_+/\tau_-$. From the analysis and direct simulation of our model, we do not find any significant dependence of the torque-speed curve characteristics on the specifics of the force function F between the load and the rotor. In particular, contrary to what was

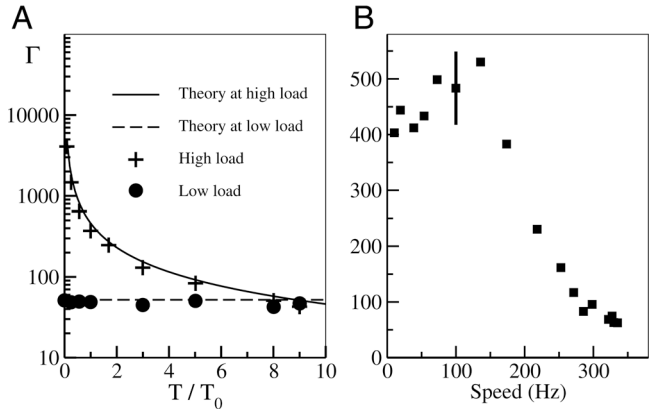

Fig. 6. The speed fluctuation and its dependence on the load (with $N = 1$). (*A*) The dependence of Γ on the external noise strength defined as T/T_0, where T_0 is the room temperature. Γ depends strongly on T for high load (crosses) while it is a constant determined by the step size at load load (dots), in agreement with our theoretical results (lines). (*B*) The dependence of Γ on speed ω for $T = T_0$. Typical error bar (SD) is shown at high load; the error at low load is comparable to the symbol size.

proposed in ref. 18, there is no difference between the case of a viscous load that interacts with the rotor through a soft spring and a viscous load without spring (see *SI Appendix*, Fig. S6 for details).

Besides the torque-speed curve that describes the time-averaged behavior of the motor, we have also studied the speed fluctuation for individual flagellar motor. We find that the fluctuation is damped by the number of stators for all load levels. However, we show that the dominating source of the motor fluctuation is different depending on the load. For low load, the speed fluctuation is dominated by the discrete stochastic stepping events, whereas, for the high load, it is controlled by the external noise, such as Brownian fluctuations or possibly measurement noises. The original measurements on motor fluctuation by Samuel and Berg (25) were done in the high-load regime as evidenced by the discrete increment of speed in their resurrection experiment. Therefore, the strength of the fluctuations obtained there is probably more reflective of the strength of external noise than the number of steps per revolution. It would be interesting to perform the fluctuation analysis in the low-load regime as achieved in ref. 19 to determine the step number per revolution and compare it with the recent direct observation of the steps (6).

Simple relations between the macroscopic observables ($\tau_{\max}, \omega_n, \omega_{\max}$) and the microscopic variables of the system (τ_0, k_+, k_-) are established by analysis of our model. These relations can be used to predict the microscopic parameters quantitatively from the torque-speed measurements. They can also be used to study the dependence of the flagellar motor properties on other relevant external parameters such as the *pmf*, the temperature, and solvent isotope effects. For example, because changing of *pmf* gives rise to self-similar torque-speed curves (30), we conclude from our model that larger *pmf* not only increases the chemical transition rates k's, it also increases the stator–rotor interaction strength τ_0. Changing temperature or replacing H^+ with D^+ (solvent isotope effect) should affect the chemical transition rates. These changes in k_+ and k_- lead to changes in the knee speed ω_n and the maximum speed $\omega_{\max}$ in our model without changing the maximum torque at stall, which is consistent with previous experimental observations (31, 32).

Backward stator jumps with $\theta^S \rightarrow \theta^S - \delta_0$ can be incorporated in our model to study the relatively rare motor back-steps (6). The back-jumps are neglected in this article because their probabilities are much smaller than those for the forward jump in the region of relative angles ($\Delta\theta > -\delta_c$) relevant for our study here. However, we expect the back-jumps to become dominant for $\Delta\theta < -\delta_c$ where the forward jumps are prohibited. Because the landing points of these back-jumps are still on the positive side of the potential with positive torque τ_0, inclusion of back-jumps in our model for $\Delta\theta < -\delta_c$ can naturally explain the observed torque continuity near stall when the motor is driven backward by an optical tweezer (9).

In our model, the step size depends inversely on the stator number N. This behavior is a general consequence of the duty ratio being unity and independent stepping of the stators, as pointed out by Samuel and Berg (25). This N^{-1} dependence of the step size seems to be inconsistent with an "apparent independence" of step size on N claimed in ref. 6. However, a careful study of the experimental data reveals that the N dependence of the step-size can not be ruled out, because the step-size distribution was measured for a varying population of stators, whose number was neither controlled nor measured precisely in ref. 6. An unambiguous way to determine whether the step size depends on N is to measure the step size for different fixed N or at least to measure N simultaneously. Such an experiment was done recently for kinesin-1 (26) and showed that step size for $N = 2$ is half of that for $N = 1$.

Our model works for the clockwise (CW) as well as for the counterclockwise (CCW) rotation. It was recently suggested that the switching between the CW and CCW state of the motor is a nonequilibrium process and the energy needed to drive the motor switch could be provided by the same *pmf* that drives the mechanical motion of the motor (33). The possible link between the switching process and the rotational motion of the motor is supported by experimental observations (10) showing that the average switching frequency depends on the proton flux. It is therefore highly desirable to develop an integrated model to describe both the mechanical part of the flagellar motor, associated with the rotational motion, with the signaling part, associated with the switching process. More experimental information on the components of the motor (M-ring/C-ring/MotAB) and how they interact with each other are needed to achieve this goal.

ACKNOWLEDGMENTS. This work was supported in part by National Science Foundation Grant CCF-0635134 (to Y.T.).

1. Berg HC, Anderson RA (1973) Bacteria swim by rotating their flagellar filaments. *Nature* 245:380–382.
2. Berg HC (2003) The rotatory motor of bacterial flagella. *Annu Rev Biochem* 72:19–54.
3. Thomas DR, Francis NR, Xu C, DeRosier DJ (2006) The Three-dimensional structure of the flagellar rotor from a clockwise-locked mutant of *Salmonella enterica* serovar Typhimurium. *J Bacteriol* 188:7039–7048.
4. Kojima S, Blair DF (2006) Conformational change in the stator of the bacterial motor. *Biochemestry* 40:13041–13050.
5. Ryu WS, Berry RM, Berg HC (2000) Torque-generating units of the flagellar motor of *Escherichia coli* have a high duty ratio. *Nature* 403:444–447.
6. Sowa Y, *et al.* (2005) Direct observation of steps in rotation of the bacterial flagellar motor. *Nature* 437:916–919.
7. Sowa Y, Hotta H, Homma M, Ishijima A (2003) Torque-speed relationship of the Na^+-driven flagellar motor of *Vibrio alginolyticus*. *J Mol Biol* 327:1043–1051.
8. Chen XC, Berg HC (2000) Torque-speed relationship of the flagellar rotatory motor of *Escherichia coli*. *Biophys J* 78:1036–1041.
9. Berry RM, Berg HC (1997) Absence of a barrier to backwards rotation of the bacterial flagellar motor demonstrated with optical tweezers. *Proc Natl Acad Sci USA* 94:14433–14437.
10. Fahrner K, Ryu WS, Berg HC (2003) Bacterial flagellar switching under load. *Nature* 423:938.
11. Reid SW, *et al.* (2006) The maximum number of torque-generating units in the flagellar motor of *Escherichia coli* is at least 11. *Proc Natl Acad Sci USA* 103:8066–8071.
12. Läuger L (1988) Torque and rotation rate of the bacterial flagellar motor. *Biophys J* 53:53–65.
13. Meister M, Caplan SR, Berg HC (1989) Dynamics of a tightly coupled mechanism for flagellar rotation. Bacterial motility, chemiosmotic coupling, protonmotive force. *Biophys J* 55:905–914.
14. Berry RM (1993) Torque and switching in the bacterial flagellar motor. An electrostatic model. *Biophys J* 64:961–973.
15. Braun TF, *et al.* (1999) Function of proline residues of MotA in torque generation by the flagellar motor of Escherichia coli. *J Bacteriol* 181:3542–3551.
16. Walz D, Caplan SR (2000) An electrostatic mechanism closely reproducing observed behavior in the bacterial flagellar motor. *Biophys J* 78:626–651.
17. Schmitt R (2003) Helix rotation model of the flagellar rotary motor. *Biophys J* 85:843–852.
18. Xing J, Bai F, Berry R, Oster G (2006) Torque-speed relationship of the bacterial flagellar motor. *Proc Natl Acad Sci USA* 103:1260–1265.
19. Yuan J, Berg HC (2008) Resurrection of the flagellar rotatory motor near zero load. *Proc Natl Acad Sci USA* 105:1182–1185.
20. Huxley AF (1957) Muscle structure and theories of contraction. *Prog Biophys Biophys Chem* 7:255–318.
21. Asbury CL, Fehr AN, Block SM (2003) Kinesin moves by asymmetric hand-over-hand mechanism. *Science* 302:2130–2134.
22. Yildiz A, Tomishige M, Vale RD, Selvin PR (2004) Kinesin walks hand-over-hand. *Science* 303:676–678.
23. Block SM, Blair D, Berg HC (1989) Compliance of bacterial flagella measured with optical tweezers. *Nature* 338:514–517.
24. Samuel ADT, Berg HC (1995) Fluctuation analysis of rotational speeds of the bacterial flagellar motor. *Proc Natl Acad Sci USA* 92:3502–3506.
25. Samuel ADT, Berg HC (1996) Torque-generating units of the bacterial flagellar motor step independently. *Biophys J* 71:918–923.
26. Leduc C, Ruhnow F, Howard J, Diaz S (2007) Detection of fractional steps in cargo movement by the collective operation of kinesin-1 motors. *Proc Natl Acad Sci USA* 104:10847–10852.
27. Blair DF, Berg HC (1988) Restoration of torque in defective flagellar motors. *Science* 242:1678–1681.
28. Visscher K, Schnitzer MJ, Block SM (1999) Single kinesin molecules studied with a molecular force clamp. *Nature* 400:184–189.
29. Oguchi Y, *et al.* (2007) Load-dependent ADP binding to myosins V and VI: Implications for subunit coordination and function. *Proc Natl Acad Sci USA* 105:7714–7719.
30. Gabel C, Berg HC (2003) The speed of the flagellar rotary motor of Escherichia coli varies linearly with protonmotive force. *Proc Natl Acad Sci USA* 100:8748–8751.
31. Berg HC, Turner L (1993) Torque generated by the flagellar motor of *Escherichia coli*. *Biophys J* 65:2201–2216.
32. Chen XC, Berg HC (2000) Solvent-Isotope and pH Effects on flagellar rotation in *Escherichia coli*. *Biophys J* 78:2280–2284.
33. Tu Y (2008) The nonequilibrium mechanism for ultrasensitivity in a biological switch: Sensing by the Maxwell's demons. *Proc Natl Acad Sci USA* 105:11737–11741.